2D Materials

RECEIVED
16 February 2015

REVISED
19 May 2015

ACCEPTED FOR PUBLICATION
29 May 2015

PUBLISHED
7 July 2015

PAPER

Strain-induced modulation of Dirac cones and van Hove singularities in a twisted graphene bilayer

V Hung Nguyen[1,2] **and P Dollfus**[1]

[1] Institut d'Electronique Fondamentale, UMR8622, CNRS, Université Paris Sud, F-91405 Orsay, France
[2] Center for Computational Physics, Institute of Physics, Vietnam Academy of Science and Technology, PO Box 429 Bo Ho, 10000 Hanoi, Vietnam

E-mail: hung@iop.vast.ac.vn

Keywords: graphene, deformation, atomistic calculation

Abstract

By means of atomistic calculations, we investigate the effects of uniaxial strain on the electronic bandstructure of a twisted graphene bilayer (T-GBL). We find that the bandstructure is dramatically deformed and the degeneracy of the bands around the Dirac points is broken by strain. As a consequence, the number of valleys in the bandstructure can double and the van Hove singularity (VHS) points are separated in energy. The dependence of these effects on the magnitude of strain, its applied direction and the twist angle is carefully examined and clarified. As an important result, we demonstrate that the position of VHSs can be modulated by strain, suggesting the possibility of observing this peculiar feature of the bandstructure at low energy in a large range of twist angles (i.e., larger than 10°). These phenomena could not be detected within the continuum approximation used in previous works. While they are in good agreement with available experimental data, our results provide a detailed understanding of the strain effects on the electronic properties of T-GBLs and may motivate further investigations of electronic transport in this type of graphene lattice.

Nowadays, graphene is one of the most attractive materials for beyond-CMOS electronics because of its specific electronic properties, which are a consequence of its two-dimensional (2D) honeycomb lattice and massless low-energy excitations, as summarized, e.g., in the review [1]. It is the basis of several peculiar phenomena and promising applications of graphene-based nanostructures [2]. Additionally, the electronic structure of graphene is relatively easy to modulate, e.g., by strain [3] or substrate [4] engineering, or by applying a perpendicular electric field [5], etc. The formation of Van der Waals heterostructures [6] has also been suggested as an effective route to control the electronic structure of graphene. Multilayer graphene, formed of graphene layers only, is one of these van der Waals structures. To modulate its electronic structure, one can rotate one graphene layer with respect to the other ones (i.e., twisted few-layer graphene) to form graphene-on-graphene moiré patterns. The twisted few-layer graphene lattices often appear in the thermal decomposition of the C-face of SiC or in the copper-assisted growth using the chemical vapor deposition method, e.g., see [7–19]. Indeed, the bandstructure in a twisted graphene bilayer (T-GBL) changes dramatically [13–19], compared to that of monolayer or Bernal/AA stacking bilayer systems. In addition to the linear dispersion in the vicinity of *K*-points, saddle points emerge at the crossing of Dirac cones (i.e., at the *M*-point in the Brillouin zone), yielding van Hove singularities (VHS) in the density of states (DOS) at low energies and remarkable renormalization of the Fermi velocity. Moreover, magnetic, optical, and phonon transport properties of the T-GBLs have a strong dependence on the twist angle [20–22]. Here, we would like to note additionally that though it has been reported theoretically that the bandstructure of Bernal stacking graphene bilayer exhibits separated 'pockets' with saddle points at low energy (i.e., a few meV around the Dirac point) when taking into account farther-neighbor interactions between two layers [23], the VHSs at these points are extremely weak and hence difficult to observe experimentally, compared to those corresponding to the bands at the *M*-point (at very high energy) [24, 25]. In this regard, since the bands at the *M*-point of slightly T-GBLs are at reasonably low energy, i.e., $\lesssim 0.5$ eV from the Dirac

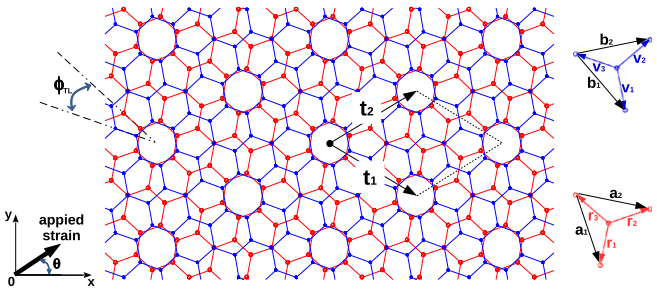

Figure 1. Schematic of twisted graphene bilayer with the twist angle ϕ_{TL} investigated in this work. $\vec{t}_{1,2}$ are its primitive vectors. The right presents two zoom images showing the nearest-neighbor vectors $\vec{r}_{1,2,3}$ ($\vec{v}_{1,2,3}$) and lattice vectors $\vec{a}_{1,2}$ ($\vec{b}_{1,2}$) of the bottom (top) layer. A uniaxial strain of angle θ with respect to the axis Ox is considered.

point for a twist angle $\phi_{TL} < 6°$ [17], the corresponding VHS points can be easily tuned/probed in practice and hence have attracted a great amount of attention [13–19]. Note that the M-point in the original Brillouin zone of monolayer or Bernal/AA stacking bilayer systems and the Brillouin zone of T-GBLs is determined similarly, i.e., as the middle point between the K and K' (i.e., Dirac) points [20].

In addition to its fascinating electronic properties, graphene also has remarkable mechanical properties. Indeed, it is able to sustain a much larger strain (i.e., >20% [26]) than any other semiconductor, making it a promising candidate for flexible electronics. Very recently, some techniques to generate extreme strain in graphene in a controlled and nondestructive way have been also explored [27, 28], so that strain engineering should become a promising approach to modulating the electronic properties of graphene nanomaterials. Many interesting electrical, optical and magnetic properties induced by strain have been actually observed [3, 29–39]. Although the bandgap of slightly strained (a few per cent) 2D graphene remains zero [40], the strain can be used to generate or strongly modulate transport gaps in some specific graphene channels, e.g., graphene nanoribbons with a local strain [30, 32], graphene with grain boundaries [31], graphene strain junctions [33, 34], and vertical devices made of twisted graphene layers [35].

The strain effects on the low-energy bands including the VHS points of Bernal stacking graphene bilayer have been widely studied as, e.g., in [41]. The bandstructure of T-GBLs has been also investigated in several works (e.g., in [13–15, 17–21, 42, 43]) using different approaches including first principles calculations, tight binding methods and continuum approximation. To the best of our knowledge, the effects of strain on VHSs in T-GBLs have been discussed only in [42, 43] and explained on the basis of calculations in the continuum approximation without taking into account the details of the atomic arrangement. This approximation has been shown to give a good description of the T-GBL bandstructure at low energy and allowed explaining the main/basic properties of VHSs observed in experiments for the slightly T-GBL without strain. However, when strain is applied, the atomic arrangement of T-GBLs is dramatically affected and becomes very strongly anisotropic, due to the strain-induced changes in C–C bond lengths. This can result in complicated deformation of graphene bandstructure, i.e., the strain effects are strongly dependent on the direction of applied strain and on the lattice orientation, as previously reported in [31, 34, 35, 40]. In particular, the strain effects on the electronic properties of two graphene sheets with different orientations should be, in principle, different. In a recent study of graphene vertical devices made of two twisted graphene layers [35], we have demonstrated that the strain can lead not only to the displacement of Dirac cones from the K-point but also to the separation of Dirac cones of the two sheets. Interestingly, this feature results in a strain-induced finite conduction gap in these vertical channels and this gap is strongly dependent on both strain amplitude and its applied direction. These properties should have a strong impact on the bandstructure of T-GBLs but they have not been fully clarified yet in the previous studies based on the continuum approximation. This raises a question about the detailed effects of strain on the bandstructure of T-GBLs when employing more accurate approaches including explicitly the arrangement of C-atoms. In this context, our aim here is to revisit this topic, i.e., the strain effects on the bandstructure of T-GBLs, using appropriate atomistic tight-binding calculations. In general, the size of supercells to consider for the atomistic simulation of a T-GBL (especially, in the cases of small twist angle) is too large for first-principles calculation, which makes the tight-binding method the most convenient, with a reasonable level of approximation. In this paper, we demonstrate several interesting features that were not clarified or even not detectable within the continuum approach used in previous works.

We investigate twisted graphene lattices consisting of two parallel graphene sheets, i.e., twisted T-GBL as schematized in figure 1. Starting from the AA stacked graphene bilayer, the rotation center was chosen at the hexagon center and then all lattices considered here

were generated by rotating one sheet with respect to the other one by a commensurate angle $\phi_{\rm TL}$. This commensurate angle is determined by $\cos\phi_{\rm TL}=(n^2/2+3mn+3m^2)/(n^2+3mn+3m^2)$ [18], where n and m are coprime positive integers. The primitive vectors of the Bravais lattice are determined as follows:

$$\begin{cases}\vec{t}_1 = m\vec{a}_1 + (n+m)\vec{a}_2,\\ \vec{t}_2 = -(n+m)\vec{a}_1 + (n+2m)\vec{a}_2,\end{cases} \quad (1)$$

if $\gcd(n,3)=1$, and

$$\begin{cases}\vec{t}_1 = \left(\frac{n}{3}+m\right)\vec{a}_1 + \frac{n}{3}\vec{a}_2,\\ \vec{t}_2 = -\frac{n}{3}\vec{a}_1 + \left(\frac{2n}{3}+m\right)\vec{a}_2,\end{cases} \quad (2)$$

if $\gcd(n,3)=3$ ($\gcd(p,q)$ is the greatest common divisor of p and q). Here, the vectors $\vec{a}_{1,2}$ are the primitive vectors of the bottom sheet as schematized in figure 1, i.e., $\vec{a}_{1,2}=\vec{r}_{1,2}-\vec{r}_3$ and their relationship with the primitive vectors $\vec{b}_{1,2}$ of the top sheet is

$$\begin{cases}\vec{b}_1 = \left(\cos\phi_{\rm TL} - \frac{\sin\phi_{\rm TL}}{\sqrt{3}}\right)\vec{a}_1 + 2\frac{\sin\phi_{\rm TL}}{\sqrt{3}}\vec{a}_2,\\ \vec{b}_2 = -2\frac{\sin\phi_{\rm TL}}{\sqrt{3}}\vec{a}_1 + \left(\cos\phi_{\rm TL} + \frac{\sin\phi_{\rm TL}}{\sqrt{3}}\right)\vec{a}_2.\end{cases} \quad (3)$$

The number of atoms in a primitive cell is $N_a = 4\left[(n+m)^2 + m(n+2m)\right]$ in the former case and $N_a = 4\left[m^2+nm+n^2/3\right]$ in the latter one. In the Oxy coordinates chosen as in figure 1, the vectors $\vec{t}_{1,2}$ of the unstrained T-GBLs can be rewritten in the following forms:

$$\vec{t}_1 = \left(3, -\sqrt{3}\right)\frac{L_0}{2} \quad \text{and} \quad \vec{t}_2 = \left(3, \sqrt{3}\right)\frac{L_0}{2}, \quad (4)$$

where $L_0 = a_0\sqrt{n^2+3nm+3m^2}$ and $a_0\sqrt{\left(n^2+3nm+3m^2\right)/3}$ for $\gcd(n,1)=1$ and 3, respectively, with the in-plane bond length a_0 (= 0.142 nm) in pristine graphene. Accordingly, the reciprocal primitive vectors of T-GBLs are given by

$$\vec{h}_1 = \left(1, -\sqrt{3}\right)\frac{2\pi}{3L_0} \quad \text{and} \quad \vec{h}_2 = \left(1, \sqrt{3}\right)\frac{2\pi}{3L_0}. \quad (5)$$

The size of the Brillouin zone in T-GBLs is hence re-scaled by a factor of a_0/L_0, compared to the original Brillouin zone in monolayer graphene (i.e., $(n,m)=(-1,1)$ and $L_0=a_0$). In the strained T-GBLs, the vectors above are all deformed due to the changes in the C–C bond lengths (see further discussions below).

To compute the electronic structure of these T-GBLs, we employed atomistic tight-binding calculations as in [15, 18–20, 33, 34, 40, 44]. A uniaxial-strain of angle θ with respect to the Ox axis is applied in the in-plane direction (see figure 1). This strain causes changes in the C–C bond vector $\vec{r}_{ij}$ according to $\vec{r}_{ij}(\sigma) = \left\{\mathbb{1} + M_{\rm strain}(\sigma,\theta)\right\}\vec{r}_{ij}(0)$ with the strain tensor

$$M_{\rm strain} = \sigma\begin{bmatrix}\cos^2\theta - \gamma\sin^2\theta & (1+\gamma)\sin\theta\cos\theta\\ (1+\gamma)\sin\theta\cos\theta & \sin^2\theta - \gamma\cos^2\theta\end{bmatrix}, \quad (6)$$

where σ represents the strain amplitude and $\gamma \simeq 0.165$ is the Poisson ratio [46]. Taking into account the strain effects, the hopping parameters were adjusted similarly as in [19, 40], i.e.

$$t_{ij}(\sigma) = \begin{cases} t_1\exp\left(-\beta_1\left\{\frac{r_{ij}(\sigma)}{a_0}-1\right\}\right)\\ \qquad \text{for in-plane couplings},\\ t_2\exp\left(-\beta_2\left\{\frac{r_{ij}(\sigma)}{d_0}-1\right\}\right)\\ \qquad \text{for interlayer couplings},\end{cases} \quad (7)$$

where $t_1=-2.7$ eV, $\beta_1=3.37$, $t_2=0.48$ eV, $\beta_2=7.42$, and $d_0=0.335$ nm. Note that due to the lattice symmetry, the bandstructures with the applied strains of angle θ and $\theta+60°$ have the same properties. Hence, our investigation is limited to $\theta\in[0°, 60°]$. Here, we especially focus on the possibility of achieving low energy saddle points. Since the bandstructure of T-GBLs is nearly symmetrical around the neutrality (Dirac) point in the considered energy range [14, 20], we only present and analyze the properties of conduction (positive-energy) bands throughout this work.

To analyze the basic properties of the bandstructure of T-GBLs under strain, we display pictures of the lowest energy bands of the lattice $\phi_{\rm TL}=9.43°$ (i.e., $n=1$ and $m=3$) without and with strain of $(\sigma,\theta)=(6\%, 20°)$ in figures 2(a) and (b), respectively. It is well known that in unstrained graphene monolayers, the first Brillouin zone has a hexagonal form with six Dirac cones at their corners. Additionally, these corners are divided into two sets of inequivalent points, i.e., K and K'. In unstrained T-GBLs, these Dirac points of two single layers are folded back to two Dirac points, K and K', in the reduced Brillouin zone [20], which is determined by the reciprocal primitive vectors in equation (5). Therefore, the Brillouin zone of T-GBLs has the same hexagonal form as that of single layers but their lowest band is composed of a pair of nearly degenerate branches around their Dirac (or K) points [20]. These two bands form two degenerate Dirac cones at the same k-point (i.e., at the K-point) as illustrated in figures 2(a) and (c). Interestingly, we find here that when a strain is applied, (i) this degeneracy can be totally lifted (see figures 2(b) and (d)) and (ii) the Dirac cones of T-GBLs are no longer located at their K-points. The latter is a general phenomenon observed for 2D graphene systems, which has been well explained by the effects of strain on the distance and hopping energies between C-atoms. The former can be explained as a consequence of the different orientations of the two graphene layers in this lattice. Basically, as reported in [31, 34], the strain-

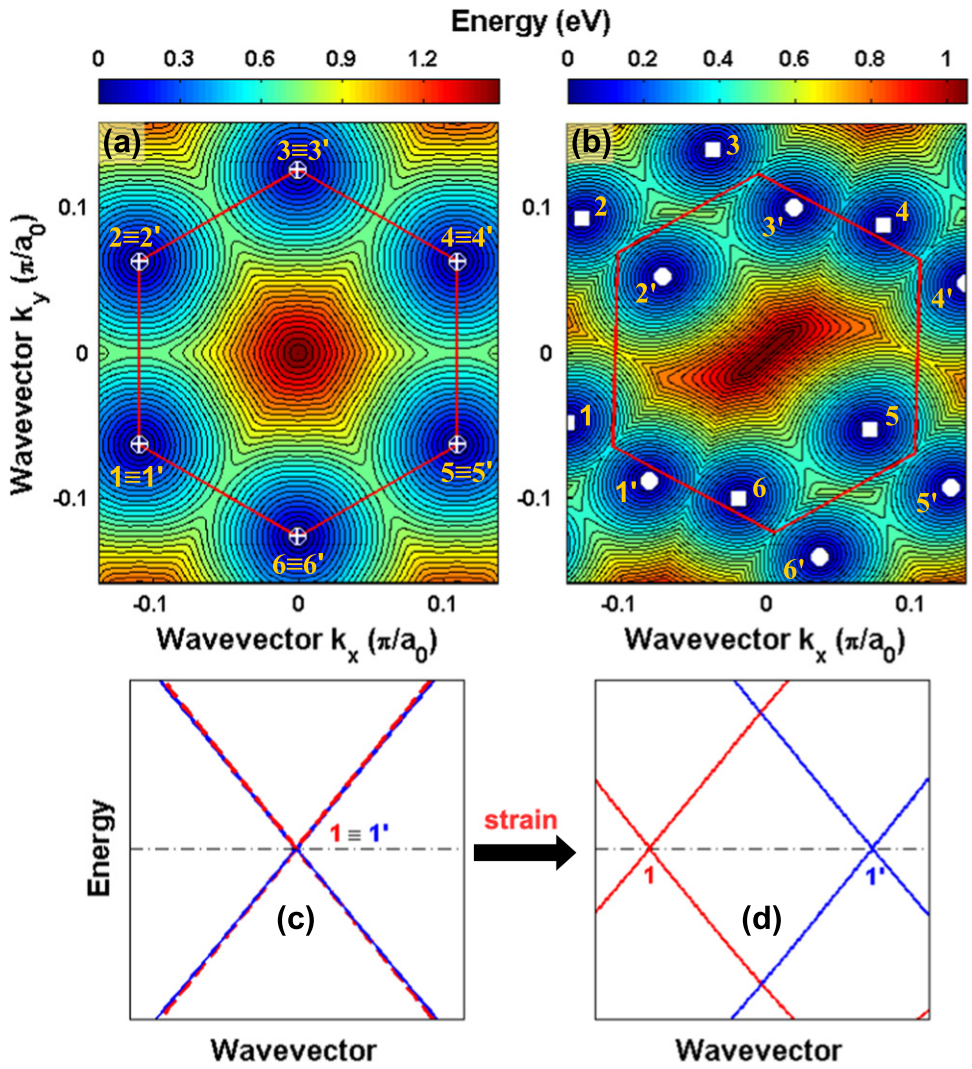

Figure 2. Map of the lowest positive-energy bands of twisted graphene bilayer without (a) and with strain (b). The twist angle $\phi_{TL} = 9.43°$ and strain of $(\sigma, \theta) = (6\%, 20°)$ are considered here. Panels (c) and (d) show schematically the strained-induced change in the bandstructure around the *K*-point.

induced deformation of the graphene bandstructure, i.e., resulting in the displacement of Dirac cones from the *K*-point, is strongly dependent on the lattice orientation. The two graphene layers in the T-GBLs have different orientations with respect to the strain direction and hence the strain effects on their bandstructure are different [35]. Though they are coupled in the T-GBLs, this difference still manifests itself in the separation of the degenerate bands around the Dirac cones and hence explains essentially our results. Here, we distinguish two groups of Dirac cones, *D* and *D*′ ($D = 1 \div 6$), which form two similar irregular hexagons and are just shifted from each other in the *k*-space (i.e., see also figure 4 and related discussions below). As a first important conclusion, the data presented in figure 2 demonstrate that the degeneracy of the bands around the Dirac cones of T-GBLs is broken and hence the number of valleys in the bandstructure of T-GBLs can double when a strain is applied. We suggest that this phenomenon can change dramatically the transport picture related to the number of valleys in graphene, e.g., valley filter and valley valve effects reported in [45]. This obtained result has not been observed yet in the previous studies based on the continuum approximation and the analysis of strain effects in the extended Brillouin zones, i.e., in the original Brillouin zones of single layers.

Next, we discuss the consequences of the phenomenon observed above on the properties of VHSs, i.e., saddle points in the bandstructure [16]. In figure 2(d), we see that the low energy bands joining the Dirac points *D* and *D*′ of the considered lattice are actually crossing bands. Therefore, even if their relative shift can occur and increase when a strain is applied, there is no saddle point between them. However, as shown in figure 3, saddle points occur close to the line joining two Dirac cones of the same group. Here, we would like to note that because of the interaction between the two layers, the bands in T-GBLs are more complex than that of single layers, especially under strain.

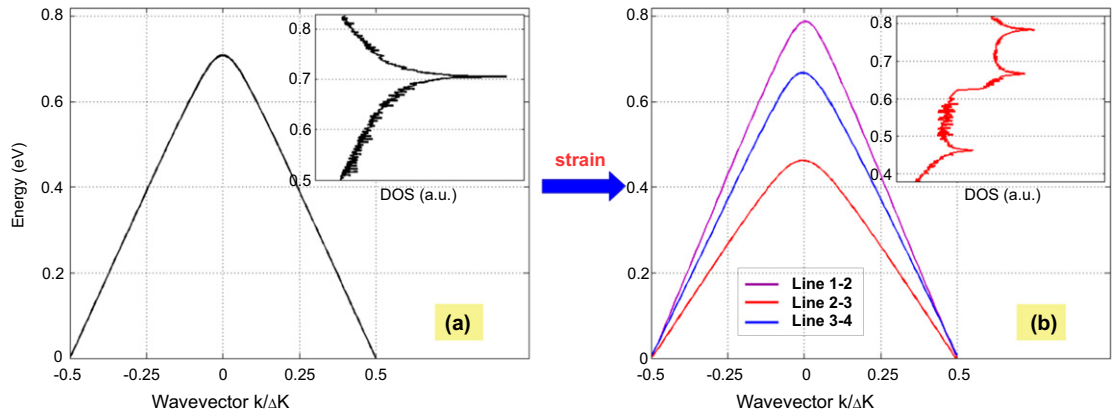

Figure 3. For the same structure and strain as in figure 2, profile of the lowest conduction band joining the Dirac points in the (a) unstrained and (b) strained cases. The insets show the DOS as a function of energy illustrating the existence of van Hove singularities.

Actually, the saddle points occur close to but not exactly on the line joining Dirac cones in the strained lattices. As discussed later, this complexity also results in difference of bandstructure properties between two different T-GBL types corresponding to gcd(n, 3) = 1 and gcd(n, 3) = 3. More importantly, we find as displayed in figure 3 that besides the separation of Dirac cones discussed above, the saddle points are also separated in energy, which is a simple consequence of the irregularity of hexagons connecting Dirac cones when the strain is applied. Note that in the unstrained lattices, these saddle points are identical, i.e., are found at the same energy (see figure 3(a)). In strained lattices, it is thus possible to achieve three different saddle points (see figure 3(b)). The existence of these saddle points is also confirmed by our plots of DOS in the insets of figure 3. We additionally observe two other features. First, compared to the unstrained case, some of the saddle points of strained T-GBLs are formed at lower energy while the others are formed at higher energy. Second, because of their separation, the peaks of DOS at these saddle points are generally smaller than that of unstrained T-GBLs. Basically, our results agree well with the experiments [43] and theoretical prediction based on the continuum approximation [42], i.e., the strain can lower the energy of saddle points. However, the energy separation of saddle points and their above properties have not been explored previously.

All phenomena observed above are of course strongly dependent on the applied strain, i.e., on its amplitude and its applied direction. Now, we would like to discuss the properties of Dirac cones and saddle points with respect to the strain direction θ. On the top of figure 4, we present two diagrams showing the position of Dirac cones (D and D') when changing θ from $-90°$ to 90°. We note again that the effects of strain angles θ and $\theta + 180°$ are identical. It is shown that when changing θ, the Dirac points move around the K-points of unstrained lattices following specific orbits. The form of hexagons D and D' connecting Dirac cones can be determined from the cone position in those orbits, according to the strain direction. Considering those orbits, we reconfirm that for the strain angles θ and $\theta + 60°$, the bands have the same properties, i.e., the hexagons in figures 4(a), (b) for the strain angle θ are identical to that for the angle $\theta + 60°$ after a rotation of 60° and a translational displacement. In figure 4(c), we plot the energy spacing between the saddle and neutrality (Dirac) points $\Delta E_{\mathrm{vHs}} = E_{\mathrm{vHs}} - E_{\mathrm{D}}$ as a function of θ for both cases of tensile ($\sigma = 6\%$) and compressive ($\sigma = -6\%$) strains. We find that (i) in all strain cases, there is at least one saddle point at lower energy than that of unstrained lattice and (ii) the saddle points have opposite properties for the tensile and compressive strains. In particular, the low energy saddle point is observed at the lowest energy for tensile strain while it is at the highest energy for compressive strain when $\theta = 30° + i60°$ and vice versa when $\theta = i60°$. Additionally, two degenerate saddle points are achieved when $\theta = i30°$. When comparing the two cases of tensile and compressive strains, it is shown that the saddle points are generally observed at higher energy in the compressive case than that in the tensile one. This can be explained by the fact that besides the deformation of the bandstructure, the hopping energies increase when the compressive strain is applied and hence the energy scale of all the bands is higher than that in the tensile case.

In the previous work [42], Chu *et al* have also investigated the effects of strain on the properties of saddle points of T-GBLs using the continuum approximation. They concluded that the tensile strain applied along the zigzag direction of the top layer (and compressive strain along the armchair direction) can lower the energy position of saddle point but the tensile strain along the armchair direction (and compressive strain along the zigzag direction) can increase it. We would like to notice that though our calculations show that the strain always lowers the smallest ΔE_{vHs}, the data in [42] are qualitatively consistent with our results displayed in figure 4(c) for the saddle point

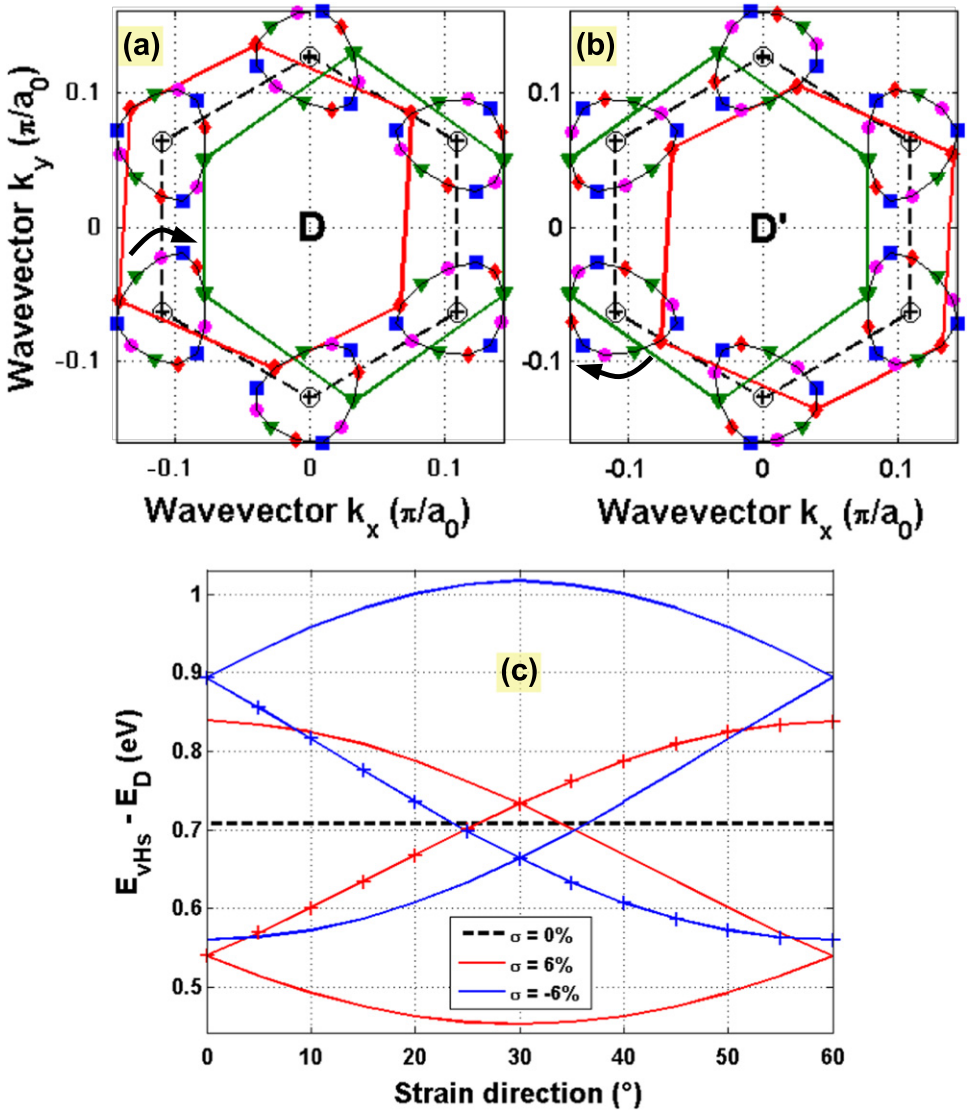

Figure 4. For the twist angle $\phi_{TL} = 9.43°$, diagrams showing the strained-induced displacement of Dirac cones (D in (a) and D' in (b), see in the text) from the K-points of unstrained lattice (circle-plus symbols) when changing the strain direction θ from $-90°$ to $90°$ with the step $\Delta\theta = 15°$. The diamond-red/triangle-green, lines correspond to $\theta = 15°$ and $\theta = 90°$ ($\equiv -90°$), respectively. (c) shows the energy spacing between van Hove singularity E_{vHs} and neutrality E_D points as a function of strain direction. The dashed line indicates the position of VHS point in the unstrain case. The strain amplitude is $\sigma = 6\%$ in (a), (b) while both tensile/compressive strains are considered in (c).

corresponding to the plus-solid line in both strain cases. The zigzag and armchair directions of top layer are actually $\theta = \phi_{TL}/2$ ($\simeq 4.72°$) and $\theta = 30° + \phi_{TL}/2$ ($\simeq 34.72°$), respectively. However, the full properties of saddle points are shown to be more complex (with three separated saddle points) than what was reported in [42].

Next, we discuss the possibilities of achieving low energy saddle points in T-GBLs by applying strain. We plot ΔE_{vHs} as a function of twist angle in the unstrained case in figure 5(a) and as a function of strain amplitude for different twisted lattices in figure 5(b). To seek for the lowest energy saddle points, the strain direction $\theta = 30°$ (resp. 0°) is considered when gcd(n, 3) = 1 (resp. 3) in figure 5(b). The difference between these two lattice types (i.e. gcd(n, 3) = 1 and 3) will be discussed later. Note that for these strain angles, there are only two saddle points in the considered energy range but they can be separated in three points for other strain directions (see figure 4(c)). First, as displayed in figure 5(a), our calculations show that for a fixed number n, ΔE_{vHs} decreases linearly when decreasing the twist angle (i.e., when increasing m), but scales differently depending on whether n is odd or even. The former property is actually in good agreement with experimental data [16, 17]. The latter can be understood as a consequence of the difference of lattice symmetry between these two cases. We notice here that similar scaling rules of $\Delta E_{vHs}(\phi_{TL})$ are also achieved when a strain is applied, as shown for instance in the data for $n = 1$ presented in figure 5(b). In the strained lattices, the saddle points are separated in energy and ΔE_{vHs} significantly decreases for low-energy saddle points while it slightly

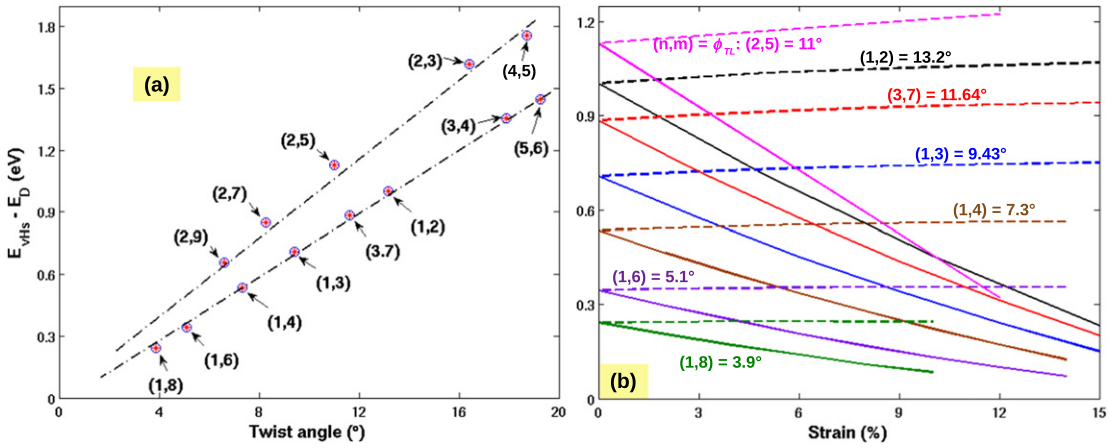

Figure 5. Energy spacing between van Hove singularity and neutrality points as a function of (a) twist angle in the unstrained case and (b) strain amplitude for different ϕ_{TL}. The numbers in brackets indicate the (n, m)-pair that fully defines the lattice (see text). The strain direction is $\theta = 30°$ (resp. 0°) when gcd$(n, 3) = 1$ (resp. 3). The solid and dashed lines in (b) correspond to the first and second saddle points, respectively.

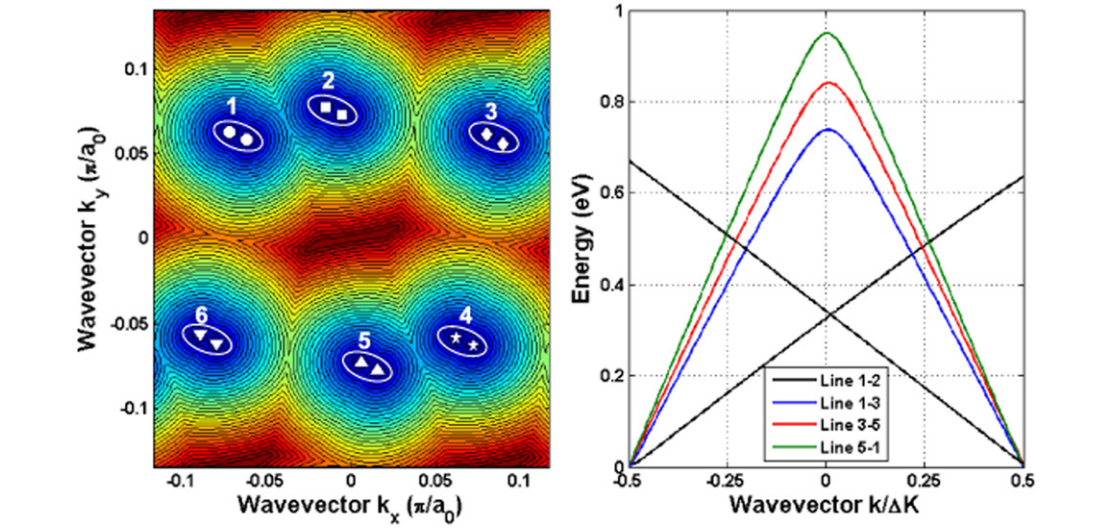

Figure 6. Map of the lowest positive-energy bands (left) and bands joining Dirac points (right) in the lattice of twist angle $\phi_{TL} = 11.64°$, i.e., with $(n, m) = (3, 7)$. The applied strain is $(\sigma, \theta) = (3\%, 15°)$.

increases for high-energy points when increasing the strain amplitude (see figure 5(b)). Interestingly, we find that for a given number n, the larger the twist angle (i.e., smaller m), the stronger the reduction of ΔE_{vHs} when increasing the strain. We suggest that this is a consequence of the folding of the bandstructure from the original bands of single layers, i.e., the band folding can weaken the effects of bandstructure deformation in slightly twisted lattices with large unit cell. More important, our results demonstrate the possibility of tuning the position of saddle points by strain [43] and of achieving low energy saddle points for a large range of ϕ_{TL}, at the expense, of course, of lower peaks of DOS, as discussed above. We would like to emphasize again that though the strain can always lower the smallest ΔE_{vHs}, this effect is strongly dependent on the strain direction, as shown in figure 4(c). Additionally, this work also suggests that multi (>1) low-energy saddle points can be obtained for moderate ϕ_{TL} and strain amplitude.

Now, we would like to clarify the specific properties of the T-GBLs with gcd$(n, 3) = 3$ detected from our calculations, which are different from the case of gcd$(n, 3) = 1$. The detailed description of the two lattice types and their difference can be found in [18]. In figure 6, we present the cartography of the lowest energy bands (left) and the bands joining Dirac points (right) for the case of $n = 3$ and $m = 7$, i.e., $\phi_{TL} = 11.64°$ in figure 5. Besides the phenomena discussed above, our calculations also show that the bandstructure of T-GBLs with gcd$(n, 3) = 3$ has dramatically different properties, compared to the cases of gcd$(n, 3) = 1$. In particular, instead of the presence of a saddle point as in the case of gcd$(n, 3) = 1$, a

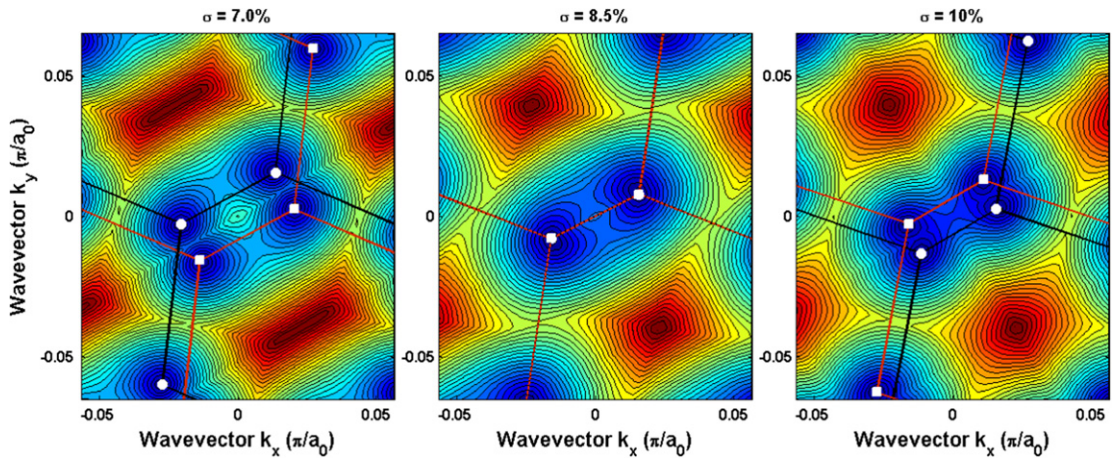

Figure 7. Map of the lowest positive-energy bands for different strains in the lattice of twist angle $\phi_{TL} = 3.9°$. The strain direction is $\theta = 30°$.

crossing of bands is observed close to the line between Dirac points of types 1 and 2. The saddle points however occur close to the lines joining the Dirac points 1–3, 3–5 and 5–1. In addition, the θ-dependence of ΔE_{vHs} in the two lattice types are also opposite, i.e., a tensile strain in the case of gcd(n, 3) = 3 (not shown) has similar effects as the compressive one for gcd(n, 3) = 1 shown in figure 4(c) and vice versa. We suggest that these differences are a direct consequence of the difference in lattice symmetries. Because of this difference, the interaction between two layers have different effects on the bandstructure when they are coupled in T-GBLs. In spite of these differences, the behavior of the VHS energy ΔE_{vHs} when increasing the strain is very similar in both lattice types, as observed in figure 5. The same feature for transport gap in the vertical devices made of two twisted graphene layers has been also observed [35].

Finally, we further investigate the bandstructure when a large strain is applied. We find, as illustrated in figure 7 for the lattice of twist angle $\phi_{TL} = 3.9°$, another interesting feature: the separation of Dirac cones in the cases of small strain can disappear when increasing the strain amplitude (for $\sigma = 8.5\%$ in this case). By further increasing the strain amplitude, this separation occurs again. This is actually a consequence of the fact that while the strain tends to displace the Dirac cones in the k-space, the size of the Brillouin zone in T-GBLs (especially, in the case of slightly twisted lattices) is much smaller than that of a single layer. Hence, the merging of Dirac cones occurs at large strain when their separation reaches the size of the Brillouin zone. The value of strain for which this merging occurs is, of course, dependent on the size of the Brillouin zone and hence on the twist angle, i.e., it increases when increasing ϕ_{TL}. This property may have an important impact on the physical phenomena related to the Dirac fermions, i.e., to the properties of Dirac cones. As an example, it should strongly influence the transport gap in vertical devices made of twisted graphene layers [35] since this gap is essentially governed by the separation of Dirac cones of the two layers in the k-space.

In conclusion, we have investigated the effects of uniaxial strain on the bandstructure of T-GBL using atomistic tight-binding calculations including the detailed arrangement of C-atoms. Compared to the previous studies based on the continuum approximation, our calculations show some new properties. In particular, the band degeneracy around the Dirac cones observed in unstrained lattices can be totally broken by strain while the bandstructure is dramatically deformed. It doubles the number of valleys and induces in the energy separation of VHS points. It is also shown that these phenomena are strongly dependent on the magnitude of strain, its applied direction, and the twist angle. Actually, the VHS points can be efficiently modulated and hence the possibility of observing this phenomenon at low energy is demonstrated in a large range of twist angles (i.e., larger than 10°) when a strain is applied in the appropriate direction. Our results provide good guidelines for exploiting the strain effects to modulate the electronic phenomena related to the properties of Dirac cones and the existence of VHSs at low energy in this type of graphene lattice.

Acknowledgments

This research in Hanoi is funded by Vietnam's National Foundation for Science and Technology Development (NAFOSTED) under grant number 103.01-2014.24.

References

[1] Castro Neto A H, Guinea F, Peres N M R, Novoselov K S and Geim A K 2009 *Rev. Mod. Phys.* **81** 109

[2] Ferrari A C *et al* 2015 *Nanoscale* **7** 4598
[3] Pereira V M and Castro Neto A H 2009 *Phys. Rev. Lett.* **103** 046801
[4] Yankowitz M, Xue J, Cormode D, Sanchez-Yamagishi J D, Watanabe K, Taniguchi T, Jarillo-Herrero P, Jacquod P and LeRoy B J 2012 *Nat. Phys.* **8** 382
[5] Zhang Y, Tang T-T, Girit C, Hao Z, Martin M C, Zettl A, Crommie M F, Shen Y R and Wang F 2009 *Nature* **459** 820
[6] Geim A K and Grigorieva I V 2013 *Nature* **499** 419
[7] de Heera W A *et al* 2007 *Solid State Commun.* **143** 92
[8] Hass J, Varchon F, Millan-Otoya J E, Sprinkle M, Sharma N, de Heer W A, Berger C, First P N, Magaud L and Conrad E H 2008 *Phys. Rev. Lett.* **100** 125504
[9] Carozo V, Almeida C M, Ferreira E H M, Cancado L G, Achete C A and Jorio A 2011 *Nano Lett.* **11** 4527
[10] Luican A, Li G, Reina A, Kong J, Nair R R, Novoselov K S, Geim A K and Andrei E Y 2011 *Phys. Rev. Lett.* **106** 126802
[11] Havener R W, Zhuang H, Brown L, Hennig R G and Park J 2012 *Nano Lett.* **12** 3162
[12] Lu C-C, Lin Y-C, Liu Z, Yeh C-H, Suenaga K and Chiu P-W 2013 *ACS Nano* **7** 2587
[13] Lopes dos Santos J M B, Peres N M R and Castro Neto A H 2007 *Phys. Rev. Lett.* **99** 256802
[14] Shallcross S, Sharma S, Kandelaki E and Pankratov O A 2010 *Phys. Rev.* B **81** 165105
[15] Trambly de Laissardière G, Mayou D and Magaud L 2010 *Nano Lett.* **10** 804
[16] Li G, Luican A, Lopes dos Santos J M B, Castro Neto A H, Reina A, Kong J and Andrei E Y 2010 *Nat. Phys.* **6** 109
[17] Brihuega I, Mallet P, González-Herrero H, Trambly de Laissardière G, Ugeda M M, Magaud L, Gómez-Rodríguez J M, Ynduráin F and Veuillen J-Y 2012 *Phys. Rev. Lett.* **109** 196802
[18] Lopes dos Santos J M B, Peres N M R and Castro Neto A H 2012 *Phys. Rev.* B **86** 155449
[19] Wang Z F, Liu F and Chou M Y 2012 *Nano Lett.* **12** 3833
[20] Moon P and Koshino M 2012 *Phys. Rev.* B **85** 195458
[21] Moon P and Koshino M 2013 *Phys. Rev.* B **88** 241412(R)
[22] Cocemasov A I, Nika D L and Balandin A A 2013 *Phys. Rev.* B **88** 035428
Cocemasov A I, Nika D L and Balandin A A 2014 *Appl. Phys. Lett.* **105** 031904
[23] McCann E and Koshino M 2013 *Rep. Prog. Phys.* **76** 056503
[24] Castro E V, López-Sancho M P and Vozmediano M A H 2009 *New J. Phys.* **11** 095017
[25] Chae D-H, Utikal T, Weisenburger S, Giessen H, Klitzing K v, Lippitz M and Smet J 2011 *Nano Lett.* **11** 1379
[26] Sharma B K and Ahn J-H 2013 *Solid-State Electron.* **89** 177
[27] Garza H H P, Kievit E W, Schneider G F and Staufer U 2014 *Nano Lett.* **14** 4107
[28] Shioya H, Craciun M F, Russo S, Yamamoto M and Tarucha S 2014 *Nano Lett.* **14** 1158
[29] Cocco G, Cadelano E and Colombo L 2010 *Phys. Rev.* B **81** 241412
[30] Lu Y and Guo J 2010 *Appl. Phys. Lett.* **97** 073105
[31] Kumar S B and Guo J 2012 *Nano Lett.* **12** 1362
[32] Bahamon D A and Pereira V M 2013 *Phys. Rev.* B **88** 195416
[33] Hung Nguyen V, Viet Nguyen H and Dollfus P 2014 *Nanotechnology* **25** 165201
[34] Chung Nguyen M, Hung Nguyen V, Viet Nguyen H and Dollfus P 2014 *Semicond. Sci. Technol.* **29** 115024
[35] Hung Nguyen V, Viet Nguyen H, Saint-Martin J and Dollfus P 2015 *Nanotechnology* **26** 115201
[36] Pereira V M, Ribeiro R M, Peres N M R and Castro Neto A H 2010 *Europhys. Lett.* **92** 67001
[37] Guinea F, Katsnelson M I and Geim A K 2010 *Nat. Phys.* **6** 30
[38] Low T and Guinea F 2010 *Nano Lett.* **10** 3551
[39] Zhai F and Yang L 2011 *Appl. Phys. Lett.* **98** 062101
[40] Pereira V M, Castro Neto A H and Peres N M R 2009 *Phys. Rev.* B **80** 045401
[41] Mucha-Kruczyński M *et al* 2011 *Phys. Rev.* B **84** 041404(R)
Mucha-Kruczyński M *et al* 2011 *Solid State Commun.* **151** 1088
Son Y-W 2011 *Phys. Rev.* B **84** 155410
[42] Chu Z-D, He W-Y and He L 2013 *Phys. Rev.* B **87** 155419
[43] Yan W, He W-Y, Chu Z-D, Liu M, Meng L, Dou R-F, Zhang Y, Liu Z, Nie J-C and He L 2013 *Nat. Commun.* **4** 2159
[44] Koshino M 2015 *New J. Phys.* **17** 015014
[45] Rycerz A, Tworzydło J and Beenakker C W J 2007 *Nat. Phys.* **3** 172
[46] Blakslee O L, Proctor D G, Seldin E J, Spence G B and Weng T 1970 *J. Appl. Phys.* **41** 3373